A Boost-Type Four-Leg Inverter With Integrated Open-Phase Fault-Tolerance for PMSM Drives

Xiaokang Zhang, Lintao Ren, Junjie Zhao, Jean-Yves Gauthier, Xuefang Lin-Shi, Fei Wang

This article has been accepted for publication in IEEE Transactions on Power Electronics. This is the author's version which has not been fully edited and content may change prior to final publication. Citation information: DOI 10.1109/TPEL.2023.3309664

A Boost-Type Four-leg Inverter with Integrated Open-Phase Fault-tolerance for PMSM Drives

Xiaokang Zhang, *Member, IEEE*, Lintao Ren, *Student Member, IEEE*, Junjie Zhao, Jean-Yves Gauthier, Xuefang Lin-Shi, and Fei Wang, *Senior Member, IEEE*

***Abstract*—This paper proposes a boost-type four-leg inverter for three-phase permanent magnet synchronous machine (PMSM) drives where the power supply is innovatively connected between the neutral point of the motor and the fourth leg. Due to the special connection, the zero-sequence circuit of a PMSM drive fed by the proposed four-leg inverter can not only be used to tolerate an open-phase fault (OPF) but also to boost the dc-bus voltage. According to the analytical modelling and equivalent circuit, it is revealed that the four-leg inverter based PMSM drive is similar to a two-stage drive under healthy operating conditions. When an OPF occurs, the motor can be normally operated with only two active phases. In post-fault conditions, the remaining phase-currents are not sinusoidal any more. Besides, the trajectory of the post-fault current vector is not a standard circle. The traditional field-oriented control strategy can still be adopted in the drive. However, the references of the d-axis current and neutral current have to be modified by injecting specific components. A differential flatness-based controller is proposed to track the time-varying current references. Experiments are carried out on a 1.2 kW PMSM test-bench to verify the effectiveness of the proposed scheme.**

***Index Terms*—Permanent magnet synchronous machine, four-leg inverter, open-phase fault, fault-tolerant control.**

I. Introduction

With the development of high-energy permanent magnet materials, permanent magnet synchronous machines (PMSMs) have been the most promising candidates for high performance industrial applications, such as electric vehicles (EVs), machine tools, air conditioners and wind power generations [1] [2]. The three-phase two-level voltage-source-inverter (VSI) has been widely used as a standard topology in most PMSM drives due to its low cost, high reliability and simple control [3]. When the voltage of a direct current (dc)-source is not high enough, the standard VSI is usually combined with a front-end dc/dc boost converter [4], namely the two-stage drive [5]. The boost converter aims at increasing and stabilizing the dc-bus voltage so that the motor can fulfill high-speed and high-efficiency operating requirements.

In actual applications, different types of faults may occur in drive systems and deteriorate the performance [6]. Some of them are related to machine windings (e.g. open-circuit or interturn short-circuit failures) and others to power converters (e.g. open/short switch faults) [7]. Normally, the short-circuit fault can be indirectly transformed to an open-circuit fault by using fuses. Thus, the open-phase fault (OPF) is recognized as one of the most common faults and received frequent attentions in motor drives [8]. Different from multi-phase [9] [10] and open-end winding [11] motors which possess the inherent fault-tolerant capability, three-phase motors require additional auxiliary components to tolerate an OPF beyond a standard VSI. Although some researchers investigated the fault-tolerant control for the standard VSI fed three-phase drives, the torque fluctuation is inevitable [12] [13]. The four-leg inverter becomes a mature fault-tolerant solution for three-phase motors which has been extensively studied in the literature. There are mainly four categories [14]–[16]: 1) capacitor-based four-leg inverter (CFI); 2) switch-based four-leg inverter (SFI); 3) capacitor-based four-leg neutral-point-connected inverter (CFNI); 4) switch-based four-leg neutral-point-connected inverter (SFNI). The CFI uses two split capacitors to replace the faulty inverter leg caused by an OPF [17]. After the fault, one of motor phases is connected to the middle point of split capacitors [18]. As a result, only half of the nominal speed can be reached in CFI. In addition, the trouble of voltage drift on the middle point of split capacitors usually affects the fault-tolerant performance. The SFI employs a redundant leg which can not only avoid the issue of voltage drift but also output the identical power rating [19] [20] in post-fault conditions. However, the cost of SFI is higher. If an OPF occurs in motor windings, both CFI and SFI are unable to tolerate it because one of motor phases is unavailable. To solve this problem, CFNI and SFNI were proposed by connecting the neutral point of motors to the midpoint of two split capacitors or a redundant inverter leg via a triode for alternating current (TRIAC), respectively [21]. In post-fault operations, the motor is rotated with only two active phases. To generate the same circular rotating magnetic field, the remaining phase-currents should be increased in magnitude by a factor of $\sqrt{3}$ and the phase angle of active phases needs to be shifted 30° away from the faulty phase [22]. As a result, the torque output capability of CFNI and SFNI is degraded by a factor of $1/\sqrt{3}$. Similar to CFI, CFNI also suffers from the trouble of voltage drift due to the use of two split capacitors. Recently, the series-end winding topology is attracting attention where the phases of a thee-phase motor are connected in series using four legs [23] [24]. The series-

Xiaokang Zhang, Lintao Ren, Junjie Zhao and Fei Wang are with the School of Mechatronic Engineering and Automation, Shanghai University, Shanghai, China (e-mail:xiaokang_zhang@shu.edu.cn; r11121572@163.com; 1105319553@shu.edu.cn; f.wang@shu.edu.cn).

Jean-Yves Gauthier and Xuefang Lin-Shi are with the Univ Lyon, INSA Lyon, Université Claude Bernard Lyon 1, Ecole Centrale de Lyon, CNRS, Ampère, UMR5005, 69621 Villeurbanne, France (e-mail:jean-yves.gauthier@insa-lyon.fr; xuefang.shi@insa-lyon.fr).

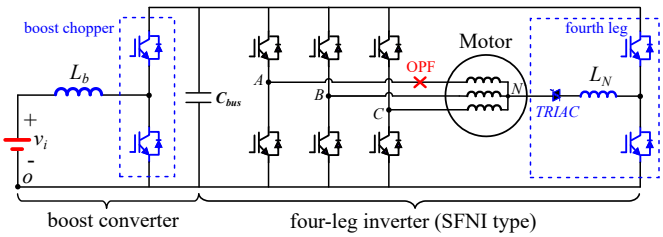

Fig. 1. Typical two-stage drive provided with the OPF fault-tolerance.

end winding topology can improve the voltage utilization and possess the fault-tolerant ability. However, the modulation method and control strategy should be modified by considering negative and zero-sequence components.

A typical two-stage drive provided with the OPF fault-tolerance is shown in Fig. 1. It consists of a frond-end dc/dc boost converter and a four-leg inverter (SFNI type). The boost chopper and the fourth leg are independent. They are responsible for the boost and the OPF fault-tolerant operations, respectively. In healthy conditions, the fourth leg and filtering inductor L_N are unoccupied, which are only put into operation when an OPF occurs by enabling the TRIAC. If the boost function and the OPF fault-tolerance can be integrated together with less power switches, the compactness of the drive can be improved. Inspired by this, a novel four-leg structure will be presented in this paper by merging the functionalities of a boost and the OPF fault-tolerance into a single four-leg inverter. The rest of this paper is organized as follows: The proposed four-leg structure is introduced and analyzed in Section II, including the modelling, equivalent circuit and characteristic analysis. In Section III, the fault-tolerant current constraints are clarified and the brand-new fault-tolerant current trajectories are proposed to maintain a stable torque. The global control strategy is presented in Section IV. Experimental results are provided in Section V. Conclusions are given in Section VI.

II. Proposed Four-leg Structure

The proposed four-leg structure is shown in Fig. 2. Compared to the typical two-stage structure, it removes the frond-end boost stage. Besides, the dc-source is connected between the neutral point of the motor and the fourth leg. The main idea of this structure is to share the fourth leg and the filtering inductor in the boost and fault-tolerant operations.

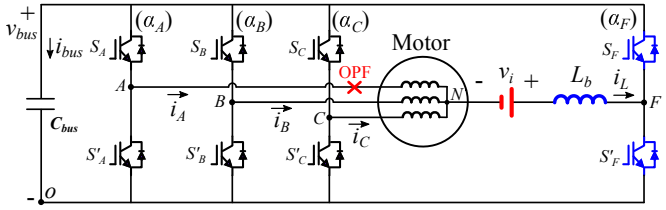

Fig. 2. Proposed four-leg inverter structure.

A. Modelling of the four-leg inverter based PMSM drive

According to Kirchhoff's Law and time-averaging equivalent approach [25], the average model of the proposed four-leg drive can be formulated with inverter's duty cycles. In A-B-C coordinate, the voltage balance equations are expressed as

$$\begin{cases} \alpha_A v_{bus} = v_{AN} + v_{NO} = v_{AN} - v_i + L_b \dfrac{\mathrm{d}i_L}{\mathrm{d}t} + \alpha_F v_{bus} \\ \alpha_B v_{bus} = v_{BN} + v_{NO} = v_{BN} - v_i + L_b \dfrac{\mathrm{d}i_L}{\mathrm{d}t} + \alpha_F v_{bus} \\ \alpha_C v_{bus} = v_{CN} + v_{NO} = v_{CN} - v_i + L_b \dfrac{\mathrm{d}i_L}{\mathrm{d}t} + \alpha_F v_{bus} \end{cases} \tag{1}$$

The current balance equations can be written as

$$\begin{cases} i_{bus} = C_{bus} \dfrac{\mathrm{d}v_{bus}}{\mathrm{d}t} = \alpha_F i_L - (\alpha_A i_A + \alpha_B i_B + \alpha_C i_C) \\ i_L = i_A + i_B + i_C \end{cases} \tag{2}$$

where v_{bus} denotes the dc-bus voltage; v_i denotes the dc-source voltage; v_{AN}, v_{BN} and v_{CN} are respectively the phase-voltages; v_{NO} indicates the neutral voltage; i_A, i_B and i_C are phase-currents; i_L is the neutral current; C_{bus} indicates the capacitance of the dc-bus capacitor; α_A, α_B, α_C and α_F represent the duty cycles of four legs; L_b is the inductance of the filtering inductor.

By applying the Park transformation (power invariant) [24] to (1) and (2), the model of the four-leg drive can be transformed from A-B-C to d-q-0 coordinates, simplified as

$$\begin{cases} \alpha_d v_{bus} = v_d = R i_d + L_d \dfrac{\mathrm{d}i_d}{\mathrm{d}t} - \omega_e L_q i_q \\ \alpha_q v_{bus} = v_q = R i_q + L_q \dfrac{\mathrm{d}i_q}{\mathrm{d}t} + \omega_e (L_d i_d + \psi_f) \\ \underbrace{(\alpha_F - \dfrac{\alpha_0}{\sqrt{3}})}_{\alpha_E} v_{bus} = -\dfrac{R}{3} i_L - \underbrace{(\dfrac{L_0}{3} + L_b)}_{L_E} \dfrac{\mathrm{d}i_L}{\mathrm{d}t} + v_i \\ i_{bus} = C_{bus} \dfrac{\mathrm{d}v_{bus}}{\mathrm{d}t} = \underbrace{(\alpha_F - \dfrac{\alpha_0}{\sqrt{3}})}_{\alpha_E} i_L - \underbrace{(\alpha_d i_d + \alpha_q i_q)}_{i_o} \end{cases} \tag{3}$$

where α_d, α_q and α_0 denote the equivalent duty cycles in d-q-0 coordinate, $\alpha_0/\sqrt{3} = (\alpha_A + \alpha_B + \alpha_C)/3$ indicates the average value of α_A, α_B and α_C; v_d, v_q and v_0 are the d-q-0 voltages; R is the stator resistance; L_d, L_q and L_0 are respectively the d-axis, q-axis and zero-sequence inductance; ω_e is the electrical angular velocity; ψ_f is the permanent magnet flux linkage; i_d and i_q are respectively the d-axis and q-axis currents; α_E, L_E and i_o are defined as new variables for simplicity.

In (3), the first two equations are the classic d-q model of a PMSM, which reveal that the PMSM can be controlled like a dc motor by regulating its flux and torque via i_d and i_q. Due to the connection of motor's neutral point, the last two equations of (3) are unique. To facilitate the understanding of the operating mechanism, an equivalent circuit will be introduced in the following.

B. Equivalent circuit

If α_E is regarded as the duty cycle of an equivalent boost chopper, we can find that the last two equations of (3) are

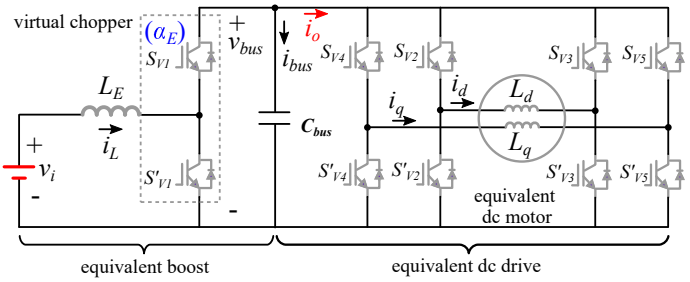

Fig. 3. Equivalent circuit of the proposed four-leg inverter fed PMSM drive.

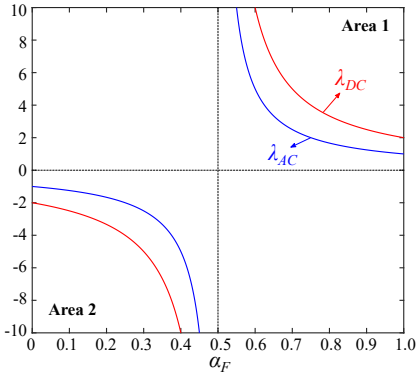

Fig. 4. Relationship of λ_{DC} and λ_{AC} with respect to α_F.

similar to the average model of a dc/dc boost converter, in which L_E is considered as the boost reactor and i_o is regarded as the load current. Accordingly, the equivalent circuit of the proposed four-leg drive is developed by visualizing the boost function, as shown in Fig. 3. A virtual boost chopper (constructed by S_{V1} and S'_{V1}) is introduced to embody the physical significance of α_E. The duty cycle of S_{V1} is α_E. L_E plays the role of a boost reactor which is constructed by $L_0/3$ and L_b. In addition, two virtual H-bridges (constructed by S_{V2}, S'_{V2}, S_{V3}, S'_{V3}, S_{V4}, S'_{V4}, S_{V5} and S'_{V5}) are introduced to reflect the physical significance of the first two equations of (3), which describes an equivalent dc motor on the d-q plane. To be specific, α_d denotes the difference between the duty cycles of S_{V2} and S_{V3}, α_q indicates the difference between the duty cycles of S_{V4} and S_{V5}. Based on above hypotheses, it is obvious that the equivalent circuit satisfies all the Kirchhoff's Law in (3). Consequently, the proposed four-leg drive is similar to a real two-stage drive in healthy conditions. Its zero-sequence circuit can be used as an equivalent boost function.

C. Steady-state characteristics

Thanks to the equivalent boost function, the dc-bus voltage can be increased. By neglecting the resistance term $(R/3)$ in (3), the step-up ratio (defined as λ_{DC}) of the equivalent boost can be expressed as

$$\lambda_{DC} = \frac{v_{bus}}{v_i} \approx \frac{1}{\alpha_E} = \frac{1}{\alpha_F - \alpha_0/\sqrt{3}} \tag{4}$$

The dc-source voltage utilization ratio (λ_{AC}) of the four-leg drive is defined as

$$\lambda_{AC} = \frac{v_{XNamp}}{v_i}, \quad X \in (A, B, C) \tag{5}$$

where v_{XNamp} is the amplitude of the phase-voltage (v_{XN}).

Because the actual duty cycle of an inverter leg is limited between 0 and 1, the attainable v_{XN} can be expressed by

$$\begin{gathered} 0 - v_{NO} \leq v_{XN} \leq v_{bus} - v_{NO} \\ \Downarrow \\ -(v_i + \alpha_F v_{bus}) \leq v_{XN} \leq v_{bus} - (v_i + \alpha_F v_{bus}) \end{gathered} \tag{6}$$

By substituting (4) into (6), we obtain

$$-\frac{\alpha_0/\sqrt{3}}{\alpha_F - \alpha_0/\sqrt{3}} v_i \leq v_{XN} \leq \frac{1 - \alpha_0/\sqrt{3}}{\alpha_F - \alpha_0/\sqrt{3}} v_i \tag{7}$$

From (7), it can be known that v_{XN} is bounded. To guarantee the symmetry of v_{XN}, $\alpha_0/\sqrt{3}$ can be set as 0.5. In this case, λ_{DC} and λ_{AC} are further formulated as

$$\begin{cases} \lambda_{DC} = \dfrac{v_{bus}}{v_i} = \dfrac{1}{\alpha_F - 0.5} \\ \lambda_{AC} = \dfrac{v_{XNamp}}{v_i} = \dfrac{0.5}{\alpha_F - 0.5} \end{cases} \tag{8}$$

According to (8), the relationship of λ_{DC} and λ_{AC} with respect to α_F is depicted in Fig. 4. In Area 1 (α_F is chosen between 0.5 and 1), both λ_{DC} and λ_{AC} are positive. When $\alpha_F = 1$, λ_{DC} and λ_{AC} are equal to 2 and 1 respectively. With the decrease of α_F, both λ_{DC} and λ_{AC} increase. This indicates that the dc-bus voltage is able to be higher than the dc-source voltage. Moreover, the boosted dc-bus voltage can effectively improve the ac voltage for the motor. This phenomenon is quite similar to a real two-stage drive with a frond-end boost converter. If v_i is connected reversely, the drive system is expected to be operated in Area 2. In this case, α_F should be chosen between 0 and 0.5.

Since the dc-source is connected with the neutral line, the input power is transferred from the neutral line to the dc-bus firstly. Then, it is consumed by the motor. In steady states, the power conservation equation can be expressed by

$$P_i = \frac{P_o}{\eta} \Rightarrow v_i i_L = \frac{T_e \omega_e}{n_{pp}\eta} = \frac{\psi_f i_q \omega_e}{\eta} \tag{9}$$

where P_i is the input power; P_o is the output power (mechanical power of the motor); η is the system efficiency; T_e is the electromagnetic torque; n_{pp} is the number of pole pairs.

According to (9), the theoretical i_L can be calculated by

$$i_L = \frac{\psi_f \omega_e i_q}{v_i \eta} = \gamma i_q \tag{10}$$

where γ is a coefficient between i_L and i_q.

III. Open-phase Fault-tolerant Operation

The fourth leg can not only be utilized as a boost chopper in healthy conditions, but also as a fault-tolerant leg when an OPF occurs. In other words, the zero-sequence path exists throughout in the proposed four-leg structure. Thus, there is no hardware switching action required from healthy to fault-tolerant conditions. For convenience, we assume that the OPF occurs in phase A. x_h and x_f denote a variable (x) in healthy and fault-tolerant conditions, respectively.

A. Post-fault current constraints

To explore the fault-tolerant potential by reusing the fourth leg, the following constraints should be considered.

Constraint 1: Torque balance

The primary objective of fault-tolerant operations is to preserve the torque of the motor. To this end, the remaining phase-currents should produce the same magnetomotive force as that in healthy conditions. For a surface-mounted PMSM, the post-fault q-axis current (i_{q_f}) should be equal to the healthy one (i_{q_h}), as

$$i_{q\_f} = i_{q\_h} \tag{11}$$

Constraint 2: Interrelationship of post-fault currents

Once the OPF occurs, i_{A_f} goes to 0 A suddenly. By considering this condition and applying Park transformation (power invariant), we obtain

$$i_{L\_f} = \sqrt{6}(i_{q\_f} sin\theta_e - i_{d\_f} cos\theta_e) \tag{12}$$

where θ_e is the electrical position.

Constraint 3: Average power balance

By combining (11) with (12), it can be predicted that i_{L_f} is not a constant but a periodic function of θ_e. This means that the instantaneous input power ($P_{i\_f} = v_i i_{L\_f}$) is changing with θ_e in post-fault conditions. If i_{d_f} is still set the same as i_{d_h}, the average value of i_{L_f} will be null over one electrical period, i.e. the average input power provided by the dc-source will be null. Obviously, this is impossible to support the motor to rotate continuously.

To achieve the fault-tolerant objective, the balance between the average input and output power should be satisfied, i.e. $< P_{i\_f} >_{\_T_f}$ should equal to P_o, which yields

$$< P_{i\_f} >_{\_T_f} = P_o \Rightarrow < i_{L\_f} >_{\_T_f} = i_{L\_h} \tag{13}$$

where T_f is the fundamental electrical period; $<>_{\_T_f}$ is an average operator over one T_f.

B. Fault-tolerant current trajectories

To fulfill the above constraints, we propose the following post-fault currents[1], as

$$\begin{cases} i_{d\_f} = i_{d\_h} - \dfrac{2}{\sqrt{6}} i_{L\_h} cos\theta_e \\ i_{q\_f} = i_{q\_h} \\ i_{L\_f} = i_{L\_h} + \sqrt{6}(i_{q\_h} sin\theta_e - i_{d\_h} cos\theta_e) + i_{L\_h} cos2\theta_e \end{cases} \tag{14}$$

Apparently, all the post-fault currents are related to their healthy states. i_{d_f} is not identical with i_{d_h}. A periodic component ($-\frac{2}{\sqrt{6}} i_{L\_h} cos\theta_e$) is superposed to i_{d_h}. i_{q_f} is absolutely the same as i_{q_h} for maintaining the torque. i_{L_f} contains a fundamental component ($\sqrt{6}(i_{q\_h} sin\theta_e - i_{d\_h} cos\theta_e)$) and a 2^{nd} component ($i_{L\_h} cos2\theta_e$) in addition to i_{L_h}.

According to (10), γ is a coefficient between i_L and i_q. It is related to the parameters of the drive system, such as the flux linkage, speed, input voltage and efficiency. For the convenience of theoretical analysis, Fig. 5 illustrates the theoretical waveforms of motor currents during a fault-tolerant transition where γ is equal to 0.5, 1 and 1.5, respectively. In healthy conditions, i_{d_h} is 0 per unit (pu) for a surface-mounted PMSM. i_{q_h} is 1 pu and i_{L_h} is equal to γ pu. The shapes of (i_{A_h}, i_{B_h} and i_{C_h}) are still sinusoidal. When the OPF occurs, i_{A_f} goes to 0 pu. To preserve the torque, i_{q_f} is remained the same as i_{q_h}. However, i_{d_f} becomes a cosine function of θ_e. i_{L_f} is not constant. It presents a unique shape due to the injected fundamental and 2^{nd} components. As a result, the shapes of remaining phase-currents (i_{B_f} and i_{C_f}) are not sinusoidal. With the increase of γ, the special shape becomes apparent. Fig. 6 illustrates the current vectors ($\boldsymbol{i_s}$) in the α-β-0 space. In healthy conditions, the current vector is still a circular with a constant zero-sequence component. In

[1]The detailed deduction of (14) is presented in Section Appendix

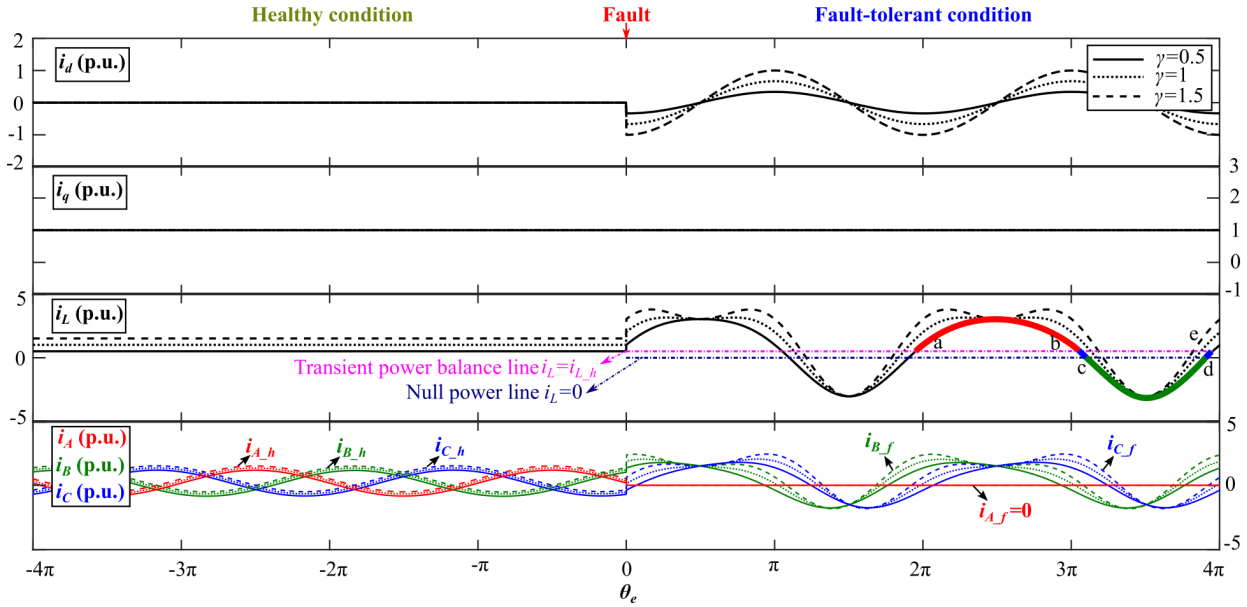

Fig. 5. Theoretical currents during a fault-tolerant transition where γ corresponds to 0.5, 1 and 1.5.

fault-tolerant conditions, it is neither a circular nor an ellipse. With the increase of γ, the shape tends to be like a heart.

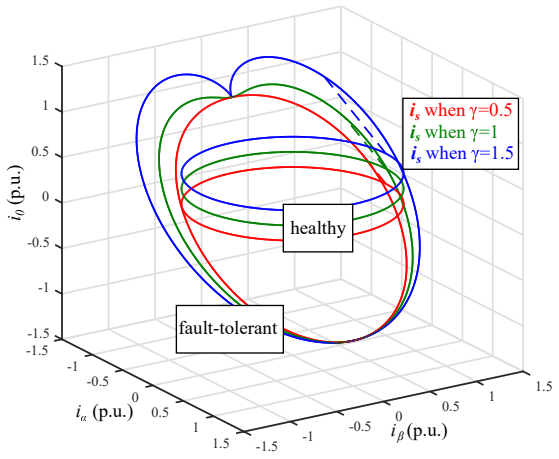

Fig. 6. Theoretical trajectories of current vectors (i_s) in healthy and fault-tolerant conditions when γ is equal to 0.5, 1 and 1.5 respectively.

C. Analysis of post-fault power conversion

Under fault-tolerant conditions, the transient input power of the drive system is time-variant because i_{L_f} is not constant. However, the transient output power of the motor is stable because the mechanical power of the motor is unchanged. Thus, the transient input power and output power are unbalanced. In this case, the dc-bus capacitor will become an energy buffer to deal with this unbalance passively.

To detail the power conversion process, i_{L_f} is divided into three segments to discuss, as shown in Fig. 5. Two lines are defined to simplify the analysis, one is called the null power line where the neutral current is 0 pu. The other is named as the transient power balance line where the neutral current is equal to i_{L_h}. Within the segments (a to b), (b to c) and (d to e), i_{L_f} is positive. This indicates that the dc-source will output energy to the system. Along with the segment (a to b), the dc-source will release more energy than what the motor can consume because the neutral current is larger than i_{L_h}. In this case, the dc-bus capacitor has to store the additional energy. As a result, the dc-bus voltage will increase. In the segments (b to c) and (d to e), the dc-source will still release energy to the system. Nevertheless, the energy is smaller than what the motor requires. In this case, the dc-bus capacitor has to fill up the energy difference. Thus, the dc-bus voltage will decrease. In the segment (c to d), the dc-source will be charged because i_{L_f} is negative. Obviously, the dc-bus voltage will also decrease during this stage. At the point 'b', the dc-bus voltage will reach its peak value. At the point 'e', it will attain its valley value. It needs to be emphasized that the mean value of the dc-bus voltage is still stable over one electrical period due to $< i_{L\_f} >_{\_T_f} = i_{L\_h}$.

IV. Global Control Strategy

According to aforementioned analysis, the proposed four-leg drive is a combination of a dc/dc boost converter and a fault-tolerant drive upon a single four-leg inverter. Thus, the control objectives of such a system include not only the motor but also the equivalent boost.

A. Brief of differential flatness theory

The differential flatness theory was introduced by Fliess *et al.* using the formalism of differential algebra [26]. The differential flatness based control is an effective means to deal with the trajectory tracking issue of nonlinear systems, which has been widely used in nonlinear dc/dc converters [27], motor drives [28] and microgrids [29].

For a nonlinear system, it can be expressed as

$$\dot{x}(t) = f(x(t), u(t)) \tag{15}$$

where $x(t) \in \mathbb{R}^n$, $u(t) \in \mathbb{R}^m$ and $(m \leq n) \in \mathbb{N}$.

The system is said to be differential flat if one can find an output y which satisfies the following smooth functions

$$\begin{aligned} h &: \mathbb{R}^n \times (\mathbb{R}^m)^{p+1} \to \mathbb{R}^m \\ \eta &: (\mathbb{R}^m)^p \to \mathbb{R}^n \\ \vartheta &: (\mathbb{R}^m)^{p+1} \to \mathbb{R}^m \end{aligned}$$

with

$$\begin{aligned} y &= h(x, u, \dot{u}, ..., u^{(p)}) \\ x &= \eta(y, \dot{y}, ..., y^{(p-1)}) \\ u &= \vartheta(y, \dot{y}, ..., y^{(p)}) \end{aligned} \tag{16}$$

where p is the order of derivatives.

In other words, the state vector x and the input vector u of a flat system can be represented by the flat output y and its derivatives. The dynamic behavior of a flat system is determined by the flat output. Once the output vector y is proved to be flat, the synthesis of a feedback control law for tracking the desired trajectory y_{traj} becomes straightforward. As depicted in Fig. 7, a flat nonlinear system can be regarded as an integral chain. Thus, the linear feedback control law ensures that the tracking error $e = y - y_{traj}$ asymptotically vanish:

$$\begin{aligned} y^{(p)} - y_{traj}^{(p)} + K_{p-1}\left[y^{(p-1)} - y_{traj}^{(p-1)}\right] + \cdots + K_0\left(y - y_{traj}\right) \\ + K_{int}\int\left(y - y_{traj}\right)\mathrm{d}t = 0 \end{aligned} \tag{17}$$

where the integral action is added to guarantee the zero steady-state error; the control gains $K_{p-1}, \cdots K_0$ and K_{int} can be chosen such that the closed-loop characteristic polynomial is $Hurwitz$. Unlike classic input-output linearization control for nonlinear systems, the flatness based control does not lead to zero dynamics. Consequently, the stability of the closed-loop system can be guaranteed.

B. Differential flatness based control for the proposed four-leg drive

Generally speaking, a motor drive is usually divided into two subsystems for its control design, one is the mechanical subsystem (low dynamic subsystem) and the other is the electrical subsystem (fast dynamic subsystem). Therefore, the mechanical dynamic can be neglected in the control design

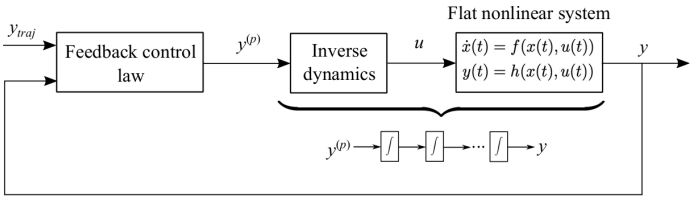

Fig. 7. Concept of the flatness based control.

of the electrical subsystem according to frequency separation principle.

For the electrical subsystem expressed in (3), the state vector $\boldsymbol{x} = [x_1, x_2, x_3, x_4]^T$ and input vector $\boldsymbol{u} = [u_1, u_2, u_3]^T$ are defined as

$$\boldsymbol{x} = [i_d, i_q, i_L, v_{bus}]^T, \quad \boldsymbol{u} = [\alpha_d, \alpha_q, \alpha_E]^T \tag{18}$$

The candidate of flat output vector $\boldsymbol{y} = [y_1, y_2, y_3]^T$ is chosen as

$$\boldsymbol{y} = [i_d, i_q, E]^T \tag{19}$$

with

$$E = \frac{1}{2}(L_d i_d^2 + L_q i_q^2 + L_E i_L^2 + C_{bus} v_{bus}^2) \tag{20}$$

where E is the energy accumulation in inductors and the dc-bus capacitor.

With this candidate $\boldsymbol{y}$, the state variables and input variables can be represented by

$$\begin{cases} x_1 = i_d = y_1 = \eta_1(y_1) \\ x_2 = i_q = y_2 = \eta_2(y_2) \\ x_3 = i_L = \dfrac{3v_i}{2R} + \\ \dfrac{\sqrt{9v_i^2 - 12R^2((i_d^2 + i_q^2) + \omega_e[\psi_f i_q + (L_d - L_q) i_d i_q + \dot{E}])}}{2R} \\ = \eta_3(y_1, y_2, \dot{y_3}) \\ x_4 = v_{bus} = \sqrt{\dfrac{2E - (L_d i_d^2 + L_q i_q^2 + L_E \eta_3^2)}{C_{bus}}} \\ = \eta_4(y_1, y_2, y_3, \dot{y_3}) \end{cases} \tag{21}$$

$$\begin{cases} u_1 = \alpha_d = \dfrac{R i_d + L_d \dot{i_d} - \omega_e L_q i_q}{\eta_4} \\ \quad = \vartheta_1(y_1, y_2, y_3, \dot{y_1}, \dot{y_3}) \\ u_2 = \alpha_q = \dfrac{R i_q + L_q \dot{i_q} + \omega_e (L_d i_d + \psi_f)}{\eta_4} \\ \quad = \vartheta_2(y_1, y_2, y_3, \dot{y_2}, \dot{y_3}) \\ u_3 = \alpha_E = \dfrac{\left[\frac{2}{9} R^2 \eta_3^2 + v_i^2 - v_i R \eta_3 - L_E(\Gamma + \ddot{E})\right]}{(v_i - \frac{2R}{3}\eta_3)\eta_4} \\ \quad = \vartheta_3(y_1, y_2, y_3, \dot{y_3}, \ddot{y_3}) \\ \text{where} \\ \Gamma = 2R(i_d \dot{i_d} + i_q \dot{i_q}) + \omega_e[\psi_f \dot{i_q} \\ \quad + (L_d - L_q) i_d \dot{i_q} + (L_d - L_q) i_q \dot{i_d}] \end{cases} \tag{22}$$

Thus, the electrical subsystem can be considered as a flat system since all the state variables and input variables are represented by the selected output vector $\boldsymbol{y}$. Then, to track the flat output trajectories (i_{d_traj}, i_{q_traj} and E_{traj}), the feedback control law is given as

$$\begin{cases} \dot{i_d} = \dot{i}_{d\_traj} - K_{d1}(i_d - i_{d\_traj}) - K_{d2} \int (i_d - i_{d\_traj})\, \mathrm{d}t \\ \dot{i_q} = \dot{i}_{q\_traj} - K_{q1}(i_q - i_{q\_traj}) - K_{q2} \int (i_q - i_{q\_traj})\, \mathrm{d}t \\ \ddot{E} = \ddot{E}_{traj} - K_{E1}(\dot{E} - \dot{E}_{traj}) - K_{E2}(E - E_{traj}) \\ \quad - K_{E3} \int (E - E_{traj})\, \mathrm{d}t \end{cases} \tag{23}$$

According to (23), the tracking errors ($e_{id} = i_d - i_{d\_traj}$, $e_{iq} = i_q - i_{q\_traj}$ and $e_E = E - E_{traj}$) yield

$$\begin{cases} \ddot{e}_{id} + K_{d1}\dot{e}_{id} + K_{d2} e_{id} = 0 \\ \ddot{e}_{iq} + K_{q1}\dot{e}_{iq} + K_{q2} e_{iq} = 0 \\ \dddot{e}_E + K_{E1}\ddot{e}_E + K_{E2}\dot{e}_E + K_{E3} e_E = 0 \end{cases} \tag{24}$$

In (24), the control parameters (K_{d1}, K_{d2}, K_{q1}, K_{q2}, K_{E1}, K_{E2} and K_{E3}) can be determined by matching desired characteristic polynomials with prespecified dynamics, as

$$\begin{cases} p_d(s) = s^2 + 2\zeta_d \omega_d s + \omega_d^2 \\ p_q(s) = s^2 + 2\zeta_q \omega_q s + \omega_q^2 \\ p_E(s) = (s + b_E)(s^2 + 2\zeta_E \omega_E s + \omega_E^2) \\ \text{with} \\ K_{d1} = 2\zeta_d \omega_d, \quad K_{d2} = \omega_d^2 \\ K_{q1} = 2\zeta_q \omega_q, \quad K_{q2} = \omega_q^2 \\ K_{E1} = b_E + 2\zeta_E \omega_E, \quad K_{E2} = 2\zeta_E \omega_E b_E + \omega_E^2 \\ K_{E3} = b_E \omega_E^2 \end{cases} \tag{25}$$

where $p_d(s)$ and $p_q(s)$ are second-order characteristic polynomials; $p_E(s)$ is a third-order characteristic polynomial; ζ_d, ζ_q and ζ_E are the desired damping ratios; ω_d, ω_q and ω_E are the nature frequencies.

The differential flatness property allows all the state and input variables to be rewritten as functions of the flat output $\boldsymbol{y}$. Therefore, the trajectories of all the state and input variables are determined by the flat output trajectory. To guarantee that all the desired trajectories are differentiable, the trajectory planning is a crucial step in the implementation of the flatness based control. A well-known waveform, such as a second-order filter can be considered so that all the transient behaviors can be predicted. In this case, the command references are reshaped by

$$\begin{cases} \dfrac{i_{d\_traj}}{i_d^*} = \dfrac{\omega_{d1}}{s^2 + 2\zeta_{d1}\omega_{d1} s + \omega_{d1}^2} \\ \dfrac{i_{q\_traj}}{i_q^*} = \dfrac{\omega_{q1}}{s^2 + 2\zeta_{q1}\omega_{q1} s + \omega_{q1}^2} \\ \dfrac{E_{\_traj}}{E^*} = \dfrac{\omega_{E1}}{s^2 + 2\zeta_{E1}\omega_{E1} s + \omega_{E1}^2} \end{cases} \tag{26}$$

where i_d^*, i_q^* and E^* are the command references; ζ_{d1}, ζ_{q1}, ζ_{E1}, ω_{d1}, ω_{q1} and ω_{E1} are respectively the desired damping ratios and nature frequencies of second-order filters.

The global control strategy of the proposed four-leg drive is depicted in Fig. 8. The typical field-oriented control is still

This article has been accepted for publication in IEEE Transactions on Power Electronics. This is the author's version which has not been fully edited and content may change prior to final publication. Citation information: DOI 10.1109/TPEL.2023.3309664

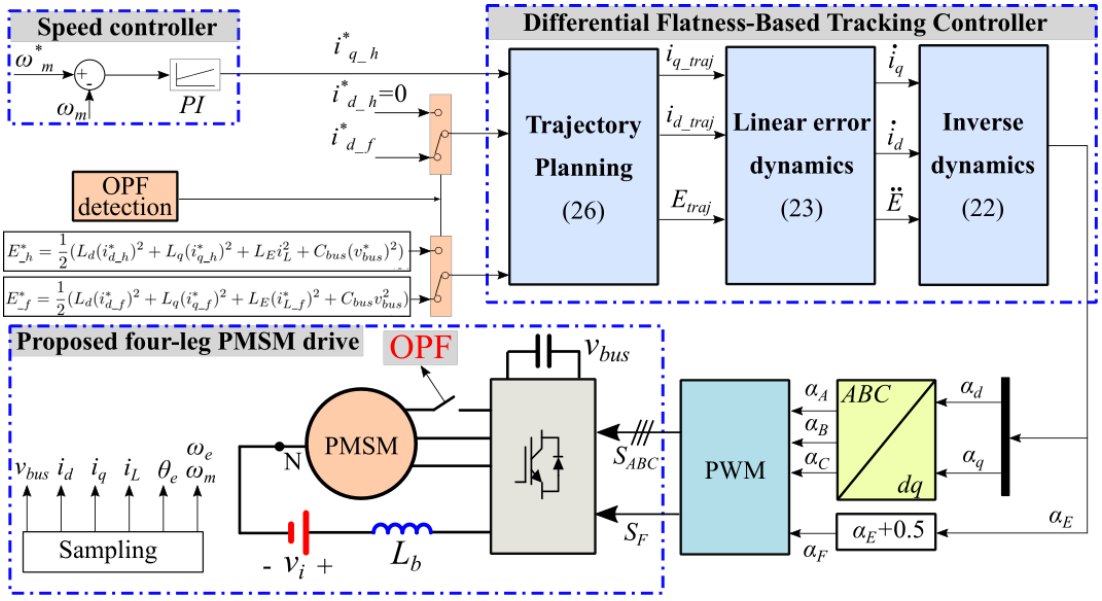

Fig. 8. Block diagram of the proposed control strategy.

adopted. In healthy conditions, ($i^*_{d\_h}$) is set as 0 for a surface-mounted PMSM. $i^*_{q\_h}$ is guided by a speed proportional integral (PI) controller. The energy reference $E^*_{\_h}$ is calculated by $E^*_{\_h} = \frac{1}{2}(L_d(i^*_{d\_h})^2 + L_q(i^*_{q\_h})^2 + L_E i_L^2 + C_{bus}(v^*_{bus})^2)$ where v^*_{bus} is the dc-bus voltage reference. Then, these references are reshaped by the trajectory planning step which generates the desired trajectories. According to the linear error dynamics, the derivatives ($\dot{i}_d$, $\ddot{i}_d$ and $\dddot{E}$) of the flat output are obtained. Then, the control inputs (α_d, α_d and α_E) are determined based on the inverse dynamics presented in (22). Then, the actual duty cycles (α_A, α_B, α_C and α_F) are calculated and applied to generate the PWM signals. Once the OPF is detected, the d-axis current reference is switched to $i^*_{d\_f}$, which can be calculated according to (14). The q-axis current reference is still remained to guarantee the torque. Regarding the energy reference, it is recalculated by $E^*_{\_f} = \frac{1}{2}(L_d(i^*_{d\_f})^2 + L_q(i^*_{q\_f})^2 + L_E(i^*_{L\_f})^2 + C_{bus}v^2_{bus})$ according to the post-fault current references.

V. Experimental Verification

Experiments are carried out on a 1.2 kW PMSM to verify the effectiveness of the proposed four-leg structure. The test-bench is shown in Fig. 9. The PMSM is a commercial product with an available neutral point. The main parameters of the motor are as follows: $L_d = L_q = 1.7$ mH; $L_0 = 2.4$ mH; $\psi_f = 0.1054$ Wb; the nominal torque is 1.2 kW; the nominal torque is 4 N·m. A 1.5 kW PMSM is used as the load motor, which is driven by an industrial inverter (LEROY SOMER). The proposed four-leg inverter is constructed with two intelligent power modules (ON Semiconductor STK581U3C2D-E). The capacitance of the dc-bus capacitor is 1880 μF. There is no additional dc-bus capacitor is employed. The inductance of L_b is 13 mH. To emulate the OPF scenario, a circuit breaker is connected in series with phase A. A current prediction based detection method is used to detect the OPF [30]. All the control algorithms are implemented on a dSPACE DS1202 MicroLabBox. The parameters of second-order filters adopted in the trajectory planning step are set as follows: $\zeta_{d1} = \zeta_{q1} = \zeta_{E1} = 1$, $\omega_{d1} = \omega_{q1} = 500$ rad/s, $\omega_E = 100$ rad/s. To avoid the overshoot effect, the feedback control law is designed by configuring the characteristic polynomials as critical damping systems, where $\zeta_d = \zeta_q = \zeta_E = 1$. The tracking dynamics is configured as five times faster than the trajectory planning dynamics, which yields $\omega_d = \omega_q = 2500$ rad/s, $\omega_E = 500$ rad/s and $b_E = 370$.

A. Validation of the equivalent boost effect

To verify the equivalent boost function, an open-loop test is firstly implemented with a 40 V dc-source. The motor here is standstill. According to aforementioned analysis, $\alpha_0/\sqrt{3} = (\alpha_A + \alpha_B + \alpha_C)/3$ should be configured as 0.5. An easy solution is to let α_A, α_B and α_C simultaneously equal to 0.5. At the beginning, α_F is set to 1. Afterwards, it is decreased

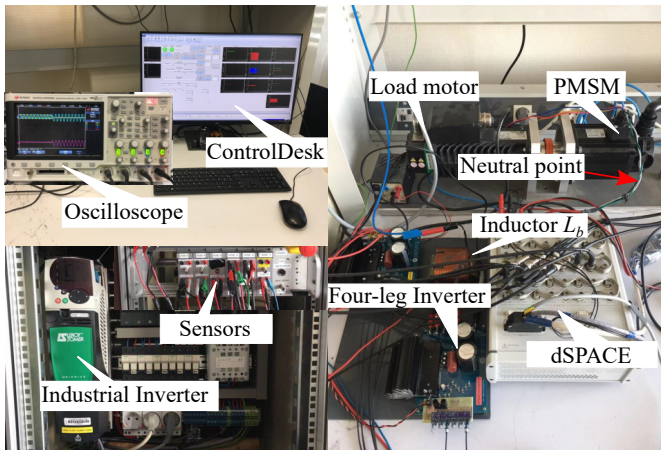

Fig. 9. Experimental test-bench.

This article has been accepted for publication in IEEE Transactions on Power Electronics. This is the author's version which has not been fully edited and content may change prior to final publication. Citation information: DOI 10.1109/TPEL.2023.3309664

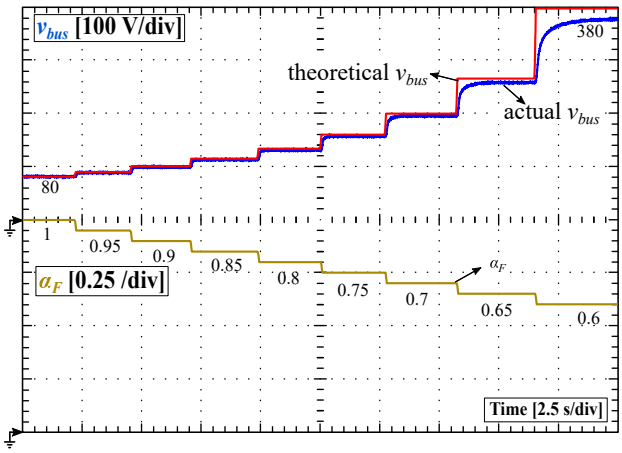

Fig. 10. Open-loop test of the equivalent boost function with a 40 V dc-source when the motor is standstill.

from 1 to 0.6 with an interval of 0.05. According to the derived step-up ratio, the theoretical v_{bus} can be calculated by $40/(\alpha_F - 0.5)$. The experimental results are illustrated in Fig. 10. It can be observed that, the actual v_{bus} can be boosted to 80 V when $\alpha_F = 1$, which is identical with the theoretical value. When α_F is decreased step by step, the actual v_{bus} can be increased. It should be noted that the actual v_{bus} shows an error with the ideal value when α_F is further decreased. The theoretical v_{bus} should be 400 V while the actual v_{bus} can only reach 380 V when α_F is 0.6. This phenomenon is caused by the effect of dead time, which is easily to be enlarged when α_F approaches to 0.5.

A startup process of the equivalent boost function is further presented in Fig. 11 under closed-loop control. In this experiment, the dc-source voltage v_i is 120 V and the reference v^*_{bus} of the dc-bus voltage is 360 V, i.e. the step-up ratio (λ_{DC}) is set to 3. Before the starting instruction, all the PWM signals are not enabled. Even so, the actual v_{bus} is exactly equal to the 120 V due to the anti-parallel diodes in the inverter. When the starting instruction is executed, v_{bus} is boosted from 120 V to 360 V. The neutral current i_L is increased from 0 A to 7 A for

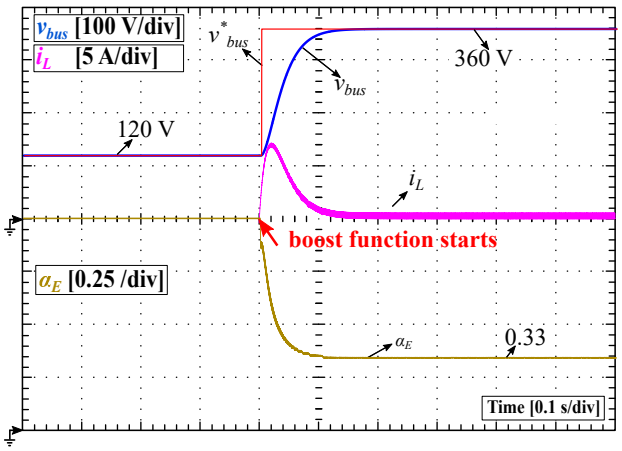

Fig. 11. A startup process of the equivalent boost function where $v_i = 120$ V and $v^*_{bus} = 360$ V.

charging the dc-bus capacitor during the startup process. When v_{bus} is regulated at 360 V stably, i_L is returned to around 0 A because the equivalent load (the motor is standstill without mechanical power) of the boost function is null. In steady states, the control input α_E is around 0.33 which is in accord with the theoretical analysis.

B. Healthy operations

Since the dc-bus voltage is boosted to 360 V, the motor is ready to rotate. To evaluate the dynamic performance of the proposed four-leg drive, acceleration, deceleration, loading and deloading tests are carried out in turn. The experimental setup is set as follows: the reference of motor's speed is 1000 rpm before 2 s. It is set to 2000 rpm at 2 s and reset to 1000 rpm at 6 s. The load torque is 1 N·m before 10 s. It is increased to 2 N·m at 10 s and released to 1 N·m again at 15 s. The experimental results are presented in Fig. 12. From Fig. 12(a), it can be seen that the actual dc-bus voltage can be well held at 360 V in different dynamic tests. Its fluctuations are up to 5 V when the speed and load torque of the motor are suddenly changed. Moreover, the motor shows a remarkable dynamic performance because it can track the speed instruct well. When the load torque is increased and decreased, the motor speed can be well maintained. The speed fluctuations

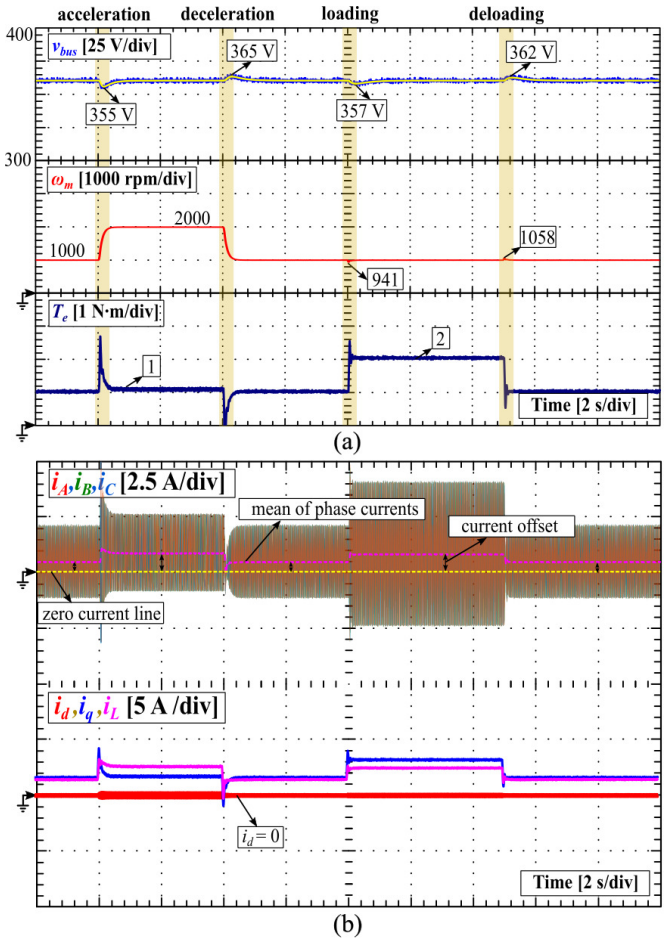

Fig. 12. Dynamic performance of the proposed four-leg drive in healthy conditions.

This article has been accepted for publication in IEEE Transactions on Power Electronics. This is the author's version which has not been fully edited and content may change prior to final publication. Citation information: DOI 10.1109/TPEL.2023.3309664

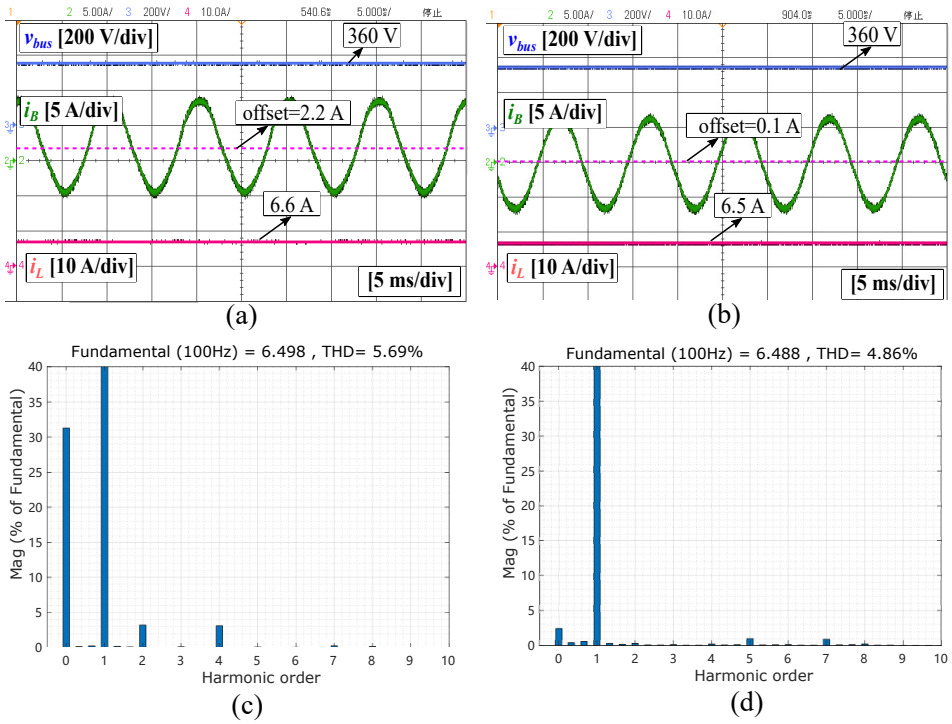

Fig. 13. Steady-state performance of the proposed four-leg drive and a typical two-stage drive with the same dc-source (120 V) and filtering inductor (L_b). (a) The dc-bus voltage, phase-B current, and neutral current of the proposed four-leg drive. (b) The dc-bus voltage, phase-B current, and inductor current of the typical two-stage drive. (c) The FFT of phase-B current in the proposed four-leg drive. (d) The FFT of phase-B current in the typical two-stage drive.

is up to 60 rpm. From Fig. 12(b), it can be seen that the phase-currents of the motor is asymmetrical. There is an offset between the zero current line and the mean of phase-currents. The offset is equal to one third of the neutral current i_L, which is proportional to the power of the motor. This is the feature of the proposed four-leg drive because its zero-sequence circuit is always conducting to play the role of the equivalent boost function.

To evaluate the steady-state performance of the proposed four-leg drive, a typical two-stage drive with the same dc-source is compared. The same filtering inductor L_b is used in the real boost stage of the two-stage drive. For both drives, the motor is operated at 1500 rpm with the rated load (4 N·m). The dc-bus voltages, phase-B currents and inductor currents of both drives are shown in Fig. 13 (a) and (b). The Fast Fourier Transform (FFT) analysis of phase-B currents is further displayed below. For the proposed four-leg drive, its dc-bus voltage can be maintained at 360 V stably like the typical two-stage drive. The phase-current shape in proposed four-leg drive is still sinusoidal. Whereas it shows an upward offset due to the connected neutral point. The offset is equal to 2.2 A, which is exactly one third of the neutral current i_L (6.6 A). In the typical two-stage drive, i_B is symmetrical with a negligible offset (0.1 A) because there is no zero-sequence current injected to the motor. The inductor currents are almost identical (6.6 A vs 6.5 A) in both drives, which means the input power of both drives is similar. Therefore, it can be concluded that the efficiency performance of the proposed four-leg inverter is not affected by the special connection of the motor's neutral point. According to the FFT results, it can be seen that the current Total Harmonic Distortion (THD) in the proposed four-leg drive is slightly increased. Compared to that in the typical two-stage drive, it is degraded by 0.83%. The zero-sequence component in the proposed four-leg drive is obviously larger than that in the two-stage drive because of the zero-sequence current. The 2^{rd} and 4^{th} harmonics are increased while the 5^{th} and 7^{th} harmonics are decreased.

C. Fault-tolerant operations

Thanks to the special connection of the neutral point, the zero-sequence path of the proposed four-leg drive can not only be used as a boost function in healthy conditions, but also as a necessary path for fault-tolerant operations. To verify the fault-tolerant possibility, a fault-tolerant transition process is recorded in Fig. 14 where the motor is operated at 1000 rpm with a 1 N·m load. At the beginning, the motor is under healthy conditions where the three phase-currents are normal and the neutral current i_L is constant. The torque of the motor is stable with the ripple of around 0.1 N·m. When the OPF occurs, i_A becomes 0 A rapidly. At that moment, the torque of the motor can not be maintained stably. It began to fluctuate with the ripple of 2 N·m. Once the fault-tolerant control is executed, the torque performance is preserved effectively with the ripple of 0.2 N·m. This verifies that the fourth leg can be reused to tolerate the OPF. The proposed current references and control strategy for fault-tolerant operations are also feasible. It needs to note that, in fault-tolerant operations, i_B and i_C are not sinusoidal and i_L is not constant. Their shapes are in accord with the theoretical curves presented in Fig. 5.

This article has been accepted for publication in IEEE Transactions on Power Electronics. This is the author's version which has not been fully edited and content may change prior to final publication. Citation information: DOI 10.1109/TPEL.2023.3309664

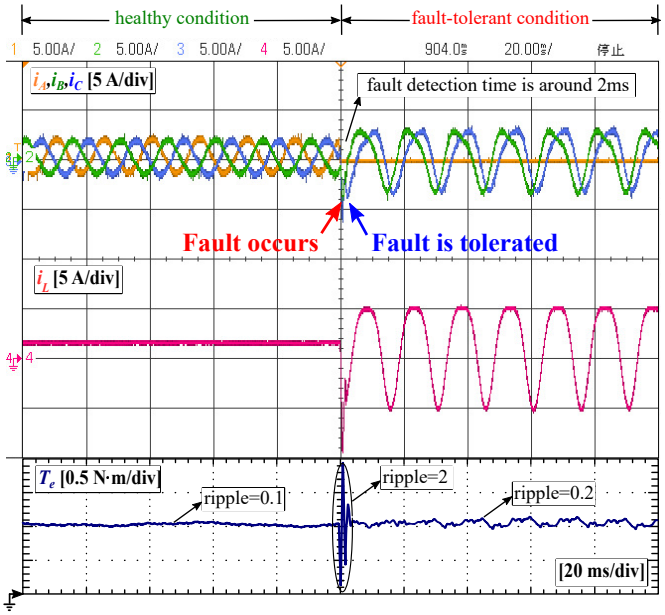

Fig. 14. A fault-tolerant transition of the proposed four-leg drive when the motor is operated at 1000 rpm with a 1 N·m load.

Fig. 15 presents the experimental results where the motor is operated at 1000 rpm with a half of the nominal load (2 N·m) in post-fault operations. Compared to Fig. 14, the special shapes of remaining phase-currents and neutral current are more noticeable. The neutral current i_L takes the shape

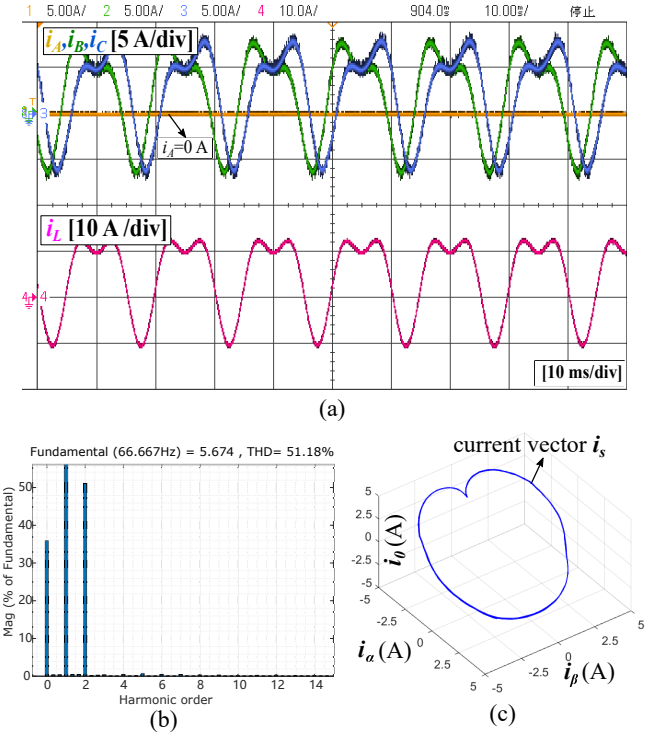

Fig. 15. Experimental results of the proposed four-leg drive in fault-tolerant operations when the motor is operated with half of the nominal torque. (a) The phase-currents and neutral current. (b) The FFT analysis of remaining phase-currents. (c) The current vector.

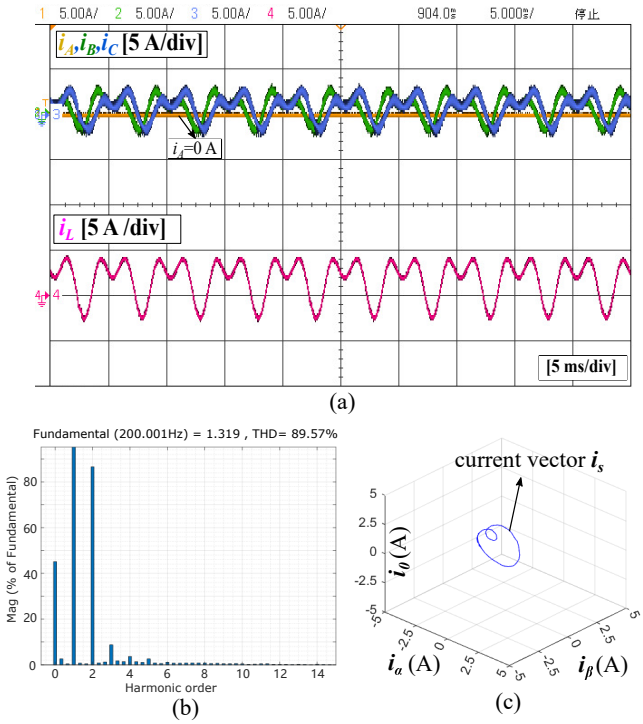

Fig. 16. Experimental results of the proposed four-leg drive in fault-tolerant operations when the motor is operated at the nominal speed. (a) The phase-currents and neutral current. (b) The FFT analysis of remaining phase-currents. (c) The current vector.

of a saddle, which is similar with the theoretical analysis presented in Fig. 5. According to the FFT result of remaining phase-currents, it can be seen that the motor contains a plenty of 2^{rd} harmonics in fault-tolerant operations. Actually, it is artificially injected to guarantee the stable torque output. The actual current vector presented in Fig. 15(c) takes the shape of a heart, which is in accord with the theoretical analysis shown in Fig. 6. This demonstrates that the proposed fault-tolerant current trajectories are effective.

To verify the fault-tolerant effectiveness when the motor is operated at the nominal speed, Fig. 16 presents the corresponding experimental results. The special shapes of remaining phase-currents and neutral current are still noticeable due to the injected components. According to the FFT analysis presented in Fig. 16(b), it can be observed that the zero-sequence component and 2^{rd} harmonics are still large due to the injected components. The THD of remaining currents is even higher than that in Fig. 15(b). This is reasonable because the value of γ is higher under high-speed conditions.

To comprehensively compare the proposed four-leg structure with the typical two-stage structure (boost + SNFI), two evaluation criteria are defined as:

- $\text{PPRF} = \dfrac{\text{maximum kVA rating under fault}}{\text{rated kVA rating in health}}$
- $\text{SOCF} = \dfrac{\text{weighted kVA rating of all silicon devices}}{\text{rated kVA rating of eight basic IGBTs}}$

The PPRF means a normalization of the maximum available power magnitude (kVA) in post-fault operations to the nominal power magnitude (kVA) under healthy conditions. The SOCF

TABLE I
COMPARISON BETWEEN THE PROPOSED FOUR-LEG INVERTER AND THE TYPICAL TWO-STAGE STRUCTURE

Topology	Integrated Boost Function	Split DC Bus	Accessible Motor Neutral	Auxiliary Silicon Components	Post-Fault Power Rating Factor (PPRF)	Silicon Overrating Cost Factor (SOCF)	Tolerate Fault Occurring in	
							Motor Side	Inverter Side
Boost+SFNI	NO	NO	YES	2 (IGBT) 1 (TRIAC)	0.58	1.87	√	√
Proposed circuit	**YES**	**NO**	YES	**null**	0.50	**1.18**	√	√

means a normalization of the weighted power magnitude (kVA) sustained by all the silicon devices under post-fault operations to the rated power magnitude (kVA) sustained by eight basic insulated-gate bipolar transistor (IGBTs) under healthy conditions. To implement this calculation, each silicon device is considered to withstand a dc-bus voltage of 1 pu and convey a phase-current RMS of 1 pu. Therefore, a healthy two-stage drive system has a SOCF of 1. To simplify the comparison, the cost of a TRIAC is assumed to be the same with an IGBT. Based on these hypotheses, the PPRF of the (boost + SNFI) is evaluated as 0.58 and the SOCF is $(3*\sqrt{3}+8)/8 = 1.65$. For the proposed four-leg structure, the PPRF is around 0.5 according to the experimental results. By neglecting the dc-component of the neutral current, the SOCF of the proposed four-leg structure can be calculated as $(2*\sqrt{3}+6)/8 = 1.18$. Consequently, compared to the (boost + SNFI) structure, the proposed circuit shows the advantage of low-cost (reduced by a factor of (1.87-1.18)/1.87=37%) with a small sacrifice on the PPRF (reduced by a factor of (0.58-0.50)/0.58=14%). A comprehensive comparison of these fault-tolerant structures is summarized in Table I.

VI. CONCLUSION

This paper proposed a novel four-leg structure for three-phase PMSM drives which integrates an equivalent boost function and the open-phase fault-tolerance upon a single four-leg inverter. The fourth leg forming the zero-sequence path is shared in the equivalent boost and fault-tolerant operations. In healthy conditions, the step-up ratio of the boost function is inversely proportional to the duty cycle of the fourth leg. Although the current THD is slightly degraded, the efficiency performance of the four-leg drive is similar as the typical two-stage drive. When an OPF occurs, the motor is able to maintain a stable torque by injecting a fundamental component to the d-axis current and a second-order harmonic to the neutral current. In post-fault operations, half of the nominal torque can be guaranteed. The remaining phase-currents are not sinusoidal and the current vector trajectory is like a heart. Theoretical analysis and experimental results have verified the effectiveness of the proposed scheme. Consequently, the proposed four-leg structure can be a promising candidate for low-cost applications. Other fault types, for example the single open-switch failure, will be further considered for the proposed four-leg inverter.

VII. APPENDIX

To maintain the torque after the fault, i_{q_f} should be equal to i_{q_h}. In this case, the sole degree of freedom is to adjust the d-axis current (i_{d_f}) by injecting a specified component. In addition, limited by the constraint of average power balance expressed in (13), the average value of the input current (neutral current i_{L_f}) under post-fault conditions should be equal to the input current (i_{L_h}) under healthy conditions. Thus, a feasible solution is to inject a periodic component ($-\frac{2}{\sqrt{6}} i_{L\_h} cos\theta_e$), as

$$i_{d\_f} = i_{d\_h} \underbrace{-\frac{2}{\sqrt{6}} i_{L\_h} cos\theta_e}_{\text{periodic component}} \tag{A.1}$$

By substituting (A.1) into (13), it is easy to obtain the expression of i_{L_f}, as

$$i_{L\_f} = i_{L\_h} + \sqrt{6}(i_{q\_h} sin\theta_e - i_{d\_h} cos\theta_e) + i_{L\_h} cos2\theta_e \tag{A.2}$$

REFERENCES

[1] K.-M. Choo and C.-Y. Won, "Design and analysis of electrical braking torque limit trajectory for regenerative braking in electric vehicles with PMSM drive systems," *IEEE Transactions on Power Electronics*, vol. 35, no. 12, pp. 13 308–13 321, dec 2020.

[2] R. Zhang, Z. Yin, N. Du, J. Liu, and X. Tong, "Robust adaptive current control of a 1.2-MW direct-drive PMSM for traction drives based on internal model control with disturbance observer," *IEEE Transactions on Transportation Electrification*, vol. 7, no. 3, pp. 1466–1481, sep 2021.

[3] S. Hu, Z. Liang, and X. He, "Ultracapacitor-battery hybrid energy storage system based on the asymmetric bidirectional Z-source topology for EV," *IEEE Transactions on Power Electronics*, vol. 31, no. 11, pp. 7489–7498, nov 2016.

[4] O. C. Onar, J. Kobayashi, and A. Khaligh, "A fully directional universal power electronic interface for EV, HEV, and PHEV applications," *IEEE Transactions on Power Electronics*, vol. 28, no. 12, pp. 5489–5498, dec 2013.

[5] A. Hota, M. Qasim, J. L. Kirtley, and V. Agarwal, "Novel boost inverter configuration and 3-ϕ induction motor drive for home appliances," in *2019 Innovations in Power and Advanced Computing Technologies (i-PACT)*. IEEE, mar 2019.

[6] X. Wang, Z. Wang, Z. Xu, M. Cheng, W. Wang, and Y. Hu, "Comprehensive diagnosis and tolerance strategies for electrical faults and sensor faults in dual three-phase PMSM drives," *IEEE Transactions on Power Electronics*, vol. 34, no. 7, pp. 6669–6684, jul 2019.

[7] A. Hajary, R. Kianinezhad, S. Seifossadat, S. Mortazavi, and A. Saffarian, "Detection and localization of open-phase fault in three-phase induction motor drives using second order rotational park transformation," *IEEE Transactions on Power Electronics*, vol. 34, no. 11, pp. 11 241–11 252, nov 2019.

[8] X. Zhou, J. Sun, H. Li, M. Lu, and F. Zeng, "PMSM open-phase fault-tolerant control strategy based on four-leg inverter," *IEEE Transactions on Power Electronics*, vol. 35, no. 3, pp. 2799–2808, mar 2020.

[9] X. Wang, Z. Wang, M. Gu, D. Xiao, J. He, and A. Emadi, "Diagnosis-free self-healing scheme for open-circuit faults in dual three-phase PMSM drives," *IEEE Transactions on Power Electronics*, vol. 35, no. 11, pp. 12 053–12 071, nov 2020.

[10] L. Zhang, X. Zhu, R. Cui, and S. Han, "A generalized open-circuit fault-tolerant control strategy for FOC and DTC of five-phase fault-tolerant permanent-magnet motor," *IEEE Transactions on Industrial Electronics*, vol. 69, no. 8, pp. 7825–7836, aug 2022.

[11] P. H. Kumar, S. Lakhimsetty, and V. T. Somasekhar, "An open-end winding BLDC motor drive with fault diagnosis and autoreconfiguration," *IEEE Journal of Emerging and Selected Topics in Power Electronics*, vol. 8, no. 4, pp. 3723–3735, dec 2020.

[12] X. Wang, Z. Wang, M. Gu, B. Wang, W. Wang, and M. Cheng, "Current optimization-based fault-tolerant control of standard three-phase PMSM drives," *IEEE Transactions on Energy Conversion*, vol. 36, no. 2, pp. 1023–1035, jun 2021.

[13] Z. Zhang, Y. Hu, G. Luo, C. Gong, X. Liu, and S. Chen, "An embedded fault-tolerant control method for single open-switch faults in standard PMSM drives," *IEEE Transactions on Power Electronics*, vol. 37, no. 7, pp. 8476–8487, jul 2022.

[14] B. Welchko, T. Lipo, T. Jahns, and S. Schulz, "Fault tolerant three-phase AC motor drive topologies: A comparison of features, cost, and limitations," *IEEE Transactions on Power Electronics*, vol. 19, no. 4, pp. 1108–1116, jul 2004.

[15] B. Mirafzal, "Survey of fault-tolerance techniques for three-phase voltage source inverters," *IEEE Transactions on Industrial Electronics*, vol. 61, no. 10, pp. 5192–5202, oct 2014.

[16] Z. Gao, C. Cecati, and S. Ding, "A survey of fault diagnosis and fault-tolerant techniques part II: Fault diagnosis with knowledge-based and hybrid/active approaches," *IEEE Transactions on Industrial Electronics*, pp. 1–1, 2015.

[17] T.-H. Liu, J.-R. Fu, and T. Lipo, "A strategy for improving reliability of field-oriented controlled induction motor drives," *IEEE Transactions on Industry Applications*, vol. 29, no. 5, pp. 910–918, 1993.

[18] K. Hu, Z. Liu, I. A. Tasiu, and T. Chen, "Fault diagnosis and tolerance with low torque ripple for open-switch fault of IM drives," *IEEE Transactions on Transportation Electrification*, vol. 7, no. 1, pp. 133–146, mar 2021.

[19] S. Bolognani, M. Zordan, and M. Zigliotto, "Experimental fault-tolerant control of a PMSM drive," *IEEE Transactions on Industrial Electronics*, vol. 47, no. 5, pp. 1134–1141, 2000.

[20] M. Tousizadeh, H. S. Che, J. Selvaraj, N. A. Rahim, and B.-T. Ooi, "Fault-tolerant field-oriented control of three-phase induction motor based on unified feedforward method," *IEEE Transactions on Power Electronics*, vol. 34, no. 8, pp. 7172–7183, aug 2019.

[21] X. Zhang, J.-Y. Gauthier, and X. Lin-Shi, "Innovative fault-tolerant three-phase SPMSM drive without split capacitors, auxiliary legs, or TRIACs," *IEEE Transactions on Power Electronics*, vol. 36, no. 7, pp. 8128–8140, jul 2021.

[22] M. Tousizadeh, H. S. Che, J. Selvaraj, N. A. Rahim, and B.-T. Ooi, "Performance comparison of fault-tolerant three-phase induction motor drives considering current and voltage limits," *IEEE Transactions on Industrial Electronics*, vol. 66, no. 4, pp. 2639–2648, apr 2019.

[23] X. Sun, Z. Liu, Z. Li, Q. Sun, A. Li, and D. Jiang, "Three-phase motor drive topology with the fault-tolerant capability of open-circuit on the multiplexing bridge," in *2021 IEEE Energy Conversion Congress and Exposition (ECCE)*. IEEE, oct 2021.

[24] X. Sun, Z. Liu, A. Li, Z. Wang, D. Jiang, and R. Qu, "Self-adaptive fault-tolerant control of three-phase series-end winding motor drive," *IEEE Transactions on Power Electronics*, vol. 37, no. 9, pp. 10 939–10 950, sep 2022.

[25] X. Zhang, J.-Y. Gauthier, X. Lin-Shi, R. Delpoux, and J.-F. Tregouet, "Modeling, control, and experimental evaluation of multifunctional converter system," *IEEE Transactions on Industrial Electronics*, vol. 68, no. 9, pp. 7747–7756, sep 2021.

[26] M. Fliess, J. Levine, P. Martin, and P. Rouchon, "A lie-backlund approach to equivalence and flatness of nonlinear systems," *IEEE Transactions on Automatic Control*, vol. 44, no. 5, pp. 922–937, may 1999.

[27] L. Gil-Antonio, B. Saldivar, O. Portillo-Rodriguez, G. Vazquez-Guzman, and S. M. D. Oca-Armeaga, "Trajectory tracking control for a boost converter based on the differential flatness property," *IEEE Access*, vol. 7, pp. 63 437–63 446, 2019.

[28] P. Thounthong, S. Sikkabut, N. Poonnoy, P. Mungporn, B. Yodwong, P. Kumam, N. Bizon, B. Nahid-Mobarakeh, and S. Pierfederici, "Nonlinear differential flatness-based speed/torque control with state-observers of permanent magnet synchronous motor drives," *IEEE Transactions on Industry Applications*, vol. 54, no. 3, pp. 2874–2884, may 2018.

[29] X. Lin-Shi, T. Simon, J.-F. Tregouet, and H. Morel, "Flatness-based control of an m-branch power flow controller for meshed DC microgrids," in *2021 IEEE 1st International Power Electronics and Application Symposium (PEAS)*. IEEE, nov 2021.

[30] A. Kontarček and P. Bajec and M. Nemec and V. Ambrožič and D. Nedeljković, "Cost-Effective Three-Phase PMSM Drive Tolerant to Open-Phase Fault," *IEEE Trans. Ind. Electron.*, vol. 62, no. 11, pp. 6708–6718, 2015.